VTT Technical Research Centre of Finland

Functionalized Nanocellulose/Multiwalled Carbon Nanotube Composites for Electrochemical Applications

Durairaj, Vasuki; Li, Panpan; Liljeström, Touko; Wester, Niklas; Etula, Jarkko; Leppänen, Ilona; Ge, Yanling; Kontturi, Katri S.; Tammelin, Tekla; Laurila, Tomi; Koskinen, Jari

Published in:
ACS Applied Nano Materials

DOI:
10.1021/acsanm.1c00774

Published: 25/06/2021

Document Version
Publisher's final version

ACS APPLIED NANO MATERIALS

www.acsanm.org Article

Functionalized Nanocellulose/Multiwalled Carbon Nanotube Composites for Electrochemical Applications

Vasuki Durairaj,* Panpan Li, Touko Liljeström, Niklas Wester, Jarkko Etula, Ilona Leppänen, Yanling Ge, Katri S. Kontturi, Tekla Tammelin, Tomi Laurila, and Jari Koskinen

Cite This: *ACS Appl. Nano Mater.* 2021, 4, 5842−5853 Read Online

ACCESS | Metrics & More | Article Recommendations | Supporting Information

ABSTRACT: Four different types of crystalline and fibrillar nanocellulosic materials with different functional groups (sulfate, carboxylate, amino-silane) are produced and used to disperse commercial multiwalled carbon nanotubes (MWCNT). Aqueous nanocellulose/MWCNT dispersions are drop-cast on tetrahedral amorphous carbon (ta-C) substrates to obtain highly stable composite electrodes. Their electrochemical properties are studied using cyclic voltammetry (CV) measurements with $Ru(NH_3)_6^{2+/3+}$, $IrCl_6^{2-/3-}$ redox probes, in electrolytes of different ionic strengths. All studied nanocellulose/MWCNT composites show excellent stability over a wide potential range (−0.6 to +1 V) in different electrolytes. Highly anionic and more porous fibrillar nanocellulosic composites indicate strong electrostatic and physical enrichment of cationic $Ru(NH_3)_6^{2+/3+}$ in lower-ionic-strength electrolytes, while lesser anionic and denser crystalline nanocellulosic composites show no such effects. This study provides essential insights into developing tailorable nanocellulose/carbon nanomaterial hybrid platforms for different electrochemical applications, by altering the constituent nanocellulosic material properties.

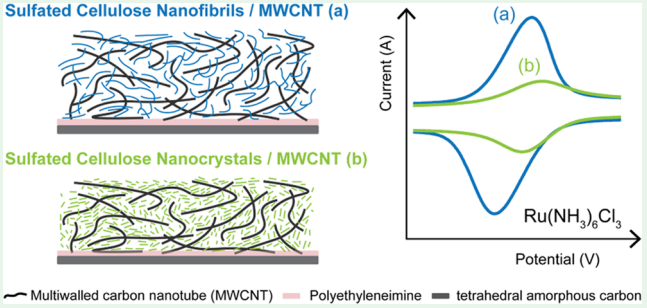

KEYWORDS: *nanocellulose, carbon nanotubes, composites, electrochemical, cyclic voltammetry, outer-sphere redox probes*

1. INTRODUCTION

The term "electrochemistry" was coined in 1814, and researchers in the 19th and 20th centuries have spearheaded tremendous advancements in the field of electrochemical applications including batteries, electroplating, mineral processing, electrolysis, and electroanalytical sensing.[1,2] Despite research interests spanning over more than two centuries, the novelty and developments in this field remain unexhausted as the advances in material processing, and especially, the development of functional nanomaterials, have given rise to several new electrochemical application fields. The main advantages of nanomaterial-based electrodes over conventional planar/bulk electrodes include higher efficiency and possibility for miniaturization, due to their large reactive surface area. Carbon nanomaterials are of particular interest in electrochemical applications owing to their often praised properties such as high electrical conductivity, chemical stability, improved reaction kinetics, and wide operation potential.[3−5]

Carbon nanomaterial-based electrodes are often developed by drop-casting, dip-coating, or printing a dispersion of the nanomaterial on top of conventional electrodes, or on polymer substrates, with conductive contact pads. The dispersions are typically prepared either by surface functionalization of the carbon nanomaterials[6] for improved stability in water or with the help of surfactants,[7] organic solvents,[8] polymers,[9] and ionic liquids.[10] These methods have certain disadvantages, such as reduction in the electrochemically active area of the carbon nanomaterial, hydrophobicity, toxicity, and high cost.

In 2012, Olivier et al.[11] showed that cellulose nanocrystals (CNC) can be used to effectively disperse single-walled carbon nanotubes (SWCNT) in aqueous colloidal suspensions. Cellulose is a linear polysaccharide abundant in all plants. Nanoscale structures, such as cellulose nanofibrils (CNF) and cellulose nanocrystals (CNC), are typically obtained by the oxidation or hydrolysis of the plant-based raw materials. This leads to the chemical functionalization of some of the numerous reactive hydroxyl groups present along the cellulose molecules. Colloidally stable aqueous dispersions of the cellulosic nanomaterials can be achieved when these surface functional groups possess sufficient ionic charge.[12−14] Such functionalized colloidally stable cellulosic nanomaterials can in turn be used to disperse carbon nanomaterials[11,15] and further offer tailorable ionic conductivity in the resultant composite matrices. In recent years, several carbon nanomaterials and other two-dimensional (2D) materials have been dispersed in

Received: March 19, 2021
Accepted: May 28, 2021
Published: June 14, 2021

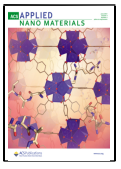

Table 1. Functionalized Nanocellulose Preparation

Raw material	Functionalization process	Ref.	Nanocellulose
Softwood dissolving cellulose pulp	Direct sulfation using a deep eutectic solvent (DES) mixture of sulfamic acid and urea, at molar ratio of 1:2, for 30 min, ended by addition of excess of water, followed by filtration and washing with water until filtrate was neutral.	36,40	Sulfated Cellulose Nanofibrils (SCNF)
Bleached birch pulp	0.1 wt% concentration of pulp subjected to TEMPO-mediated oxidation with addition of 5.0 mmol NaClO (per gram of pulp) at room temp. and pH 10, for 130 min, followed by washing with deionized water.	37,41	TEMPO-Oxidized Cellulose Nanofibrils (TOCNF)
Cotton cellulose paper	Sulfuric acid hydrolysis with 64% w/w sulfuric acid at 45 °C for 45 min, followed by counterion exchange with 0.1 M NaOH until pH neutralized.	38,42	Sulfated Cellulose Nanocrystals (SCNC)
Commercial CNC powder (CelluForce NCC®) from CelluForce (Canada)	Purification of CNC powder by Soxhlet extraction (with ethanol). Purified CNC dispersed in dimethyl-acetamide/ lithium chloride solution, (mass ratio 99:1) to get 1 wt % CNC suspension. 3.33 ml of APTMS added to dispersion and reaction carried out first at 80 °C for 2 hours, then at room temperature for 12 hours, followed by dialysis in milliQ water for 4 days.	39,43	Amino – silanized Cellulose Nanocrystals (ACNC)

nanocellulosic matrices to obtain functional hybrid nanocomposites for various applications.[16−22] We have previously demonstrated that the presence of a high density of negatively charged sulfate functional groups on the nanocellulose can significantly improve the selectivity of multiwalled carbon nanotubes (MWCNTs) in the composite electrode, toward the cationic dopamine molecule.[23] The use of such nanocellulose/nanocarbon composites in electrochemical applications has become increasingly popular in the recent years.[24−30] However, this field is still very much at its early stages, and there is a lack of systematic studies regarding the effects of the nanocellulosic material properties, upon the electrochemical performance of such composites.

In this study, we produce four different nanocellulosic materials, namely, sulfated cellulose nanofibrils (SCNF), TEMPO (2,2,6,6-tetramethylpiperidin-1-oxyl)-mediated oxidized cellulose nanofibrils (TOCNF), sulfated cellulose nanocrystals (SCNC), and APTMS ((3-aminopropyl) trimethoxysilane)-mediated amino-silanized cellulose nanocrystals (ACNC). The choice of such vastly different nanocellulose functionalization chemistries and starting materials is intentional, to investigate (i) the efficacy of such a wide range of nanocellulosic materials in dispersing MWCNT and (ii) the nanocellulose-dependent variations in the electrochemical properties of the resultant composites. Aqueous suspensions of the functionalized nanocellulosic materials are used to disperse commercial MWCNT. Pure nanocellulosic materials, without any functional groups cannot be included for investigation in this work, as the extraction of nanocellulosic structures from plant-based sources involves processes that introduce surface functional groups on the cellulose molecules, and removal of such functional groups would result in immediate aggregation of the nanofibers or nanocrystals.

We characterize the functionalized nanocellulosic materials and the corresponding nanocellulose/MWCNT dispersions using standard chemical and physical characterization methods, to establish successful functionalization of the nanocellulosic materials and to verify the MWCNT dispersion. The different nanocellulose/MWCNT suspensions are drop-cast on top of tetrahedral amorphous carbon (ta-C) thin-film-coated silicon wafer pieces. ta-C thin films are versatile, chemically inert coatings that can be made using low-cost, patternable, and complementary metal−oxide−semiconductor (CMOS)-compatible, room-temperature deposition process on a variety of substrates.[31,32] Modification of the ta-C electrodes with high-surface-area carbon nanomaterials has been shown to significantly improve sensitivity and offer tailorable selectivity toward various small biomolecules for sensing applications.[23,33−35]

Electrochemical properties of the drop-cast nanocellulose/MWCNT composites are investigated using cyclic voltammetry (CV) measurements with $Ru(NH_3)_6^{2+/3+}$, $IrCl_6^{2-/3-}$ outer-sphere redox (OSR) probes, in 10 mM phosphate buffer saline (PBS) solution, and 1 M KCl. CVs of all four types of nanocellulose/MWCNT composites show excellent stability for 100 cycles at 500 mV/s scan rate, over a wide potential range (−0.6 to +1 V) in both PBS and KCl. Electrochemical responses of the cationic $Ru(NH_3)_6^{2+/3+}$ probe at different electrode types are highly varied, indicating strong physical and electrostatic effects dependent on the constituent nanocellulosic material properties, as well as the ionic strength of the supporting electrolyte. Such tailorable morphological and electrostatic effects, combined with excellent electrode stabilities, are highly promising for different electrochemical applications. The physicochemical characterizations in this study, together with the electrochemical investigations, correlate the nanocellulose dimensions and surface functionalizations to the electrochemical performance of resultant nanocellulose/MWCNT composite platforms and provide

https://doi.org/10.1021/acsanm.1c00774
ACS Appl. Nano Mater. 2021, 4, 5842−5853

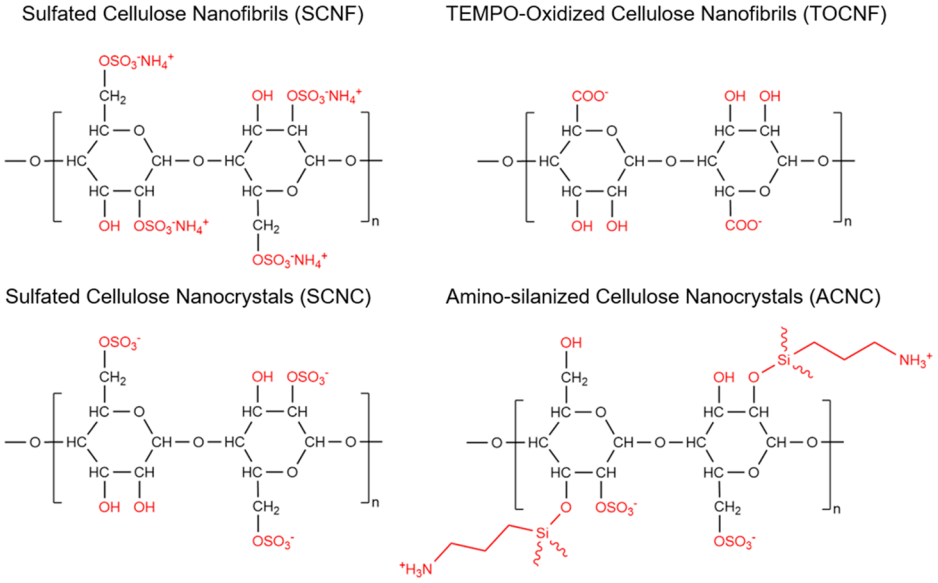

Figure 1. Chemical structures of functionalized nanocellulosic materials (ChemDraw 19.1).

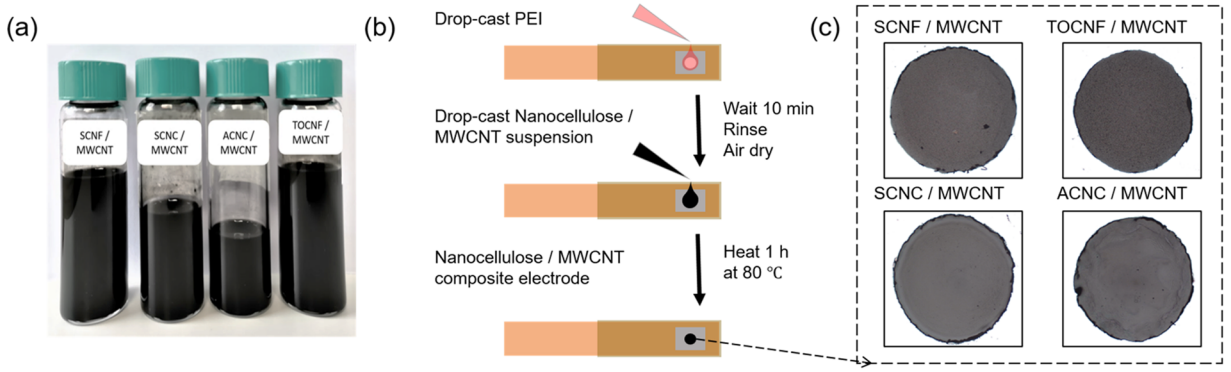

Figure 2. (a) Photograph of different nanocellulose/MWCNT suspensions. (b) Schematic of electrode preparation. (c) Optical microscope images of drop-cast composite electrodes.

essential insights into designing such hybrid electrode materials for various applications.

2. EXPERIMENTAL SECTION

2.1. Functionalized Nanocellulosic Materials Preparation. Four different nanocellulosic materials, namely, SCNF, TOCNF, SCNC, and ACNC, were prepared using processes based on previously published works by Sirviö et al.,[36] Saito et al.,[37] Dong et al.,[38] and Arola et al.,[39] respectively. The preparation processes are briefly tabulated in Table 1. Simplified chemical structures of the different functionalized nanocellulosic materials are shown in Figure 1. The functionalized nanocellulose suspensions were diluted to 0.25 wt % in Milli-Q water and stored in a refrigerator at ∼5 °C.

2.2. Preparation of Functionalized Nanocellulose/MWCNT Dispersions. Multiwalled carbon nanotubes were purchased from NanoLab, Inc. (Newton, MA) in dry powder form. The MWCNTs were grown by chemical vapor deposition (CVD) process (purity > 95%) and are specified to have outer diameters in the range of 30 ± 15 nm and lengths of 5−20 μm. The MWCNTs were used as received, without any pretreatments. Dispersions of functionalized nanocellulosic materials with MWCNT were prepared by adding 0.125 wt % (0.0125 g) of dry MWCNT to 10 g of the 0.25 wt % aqueous nanocellulose suspension (final dry weight ratio of nanocellulose/MWCNT = 2:1). The resulting mixtures were tip-sonicated in an ice bath, using a Qsonica Q500 tip sonicator, with a 2 mm probe at 20 kHz (30 W), for 10 min in pulsed mode (5 s on and 1 s off). The total energy delivered to each nanocellulose/MWCNT suspension was 18 000 J. Tip sonication parameters were chosen to ensure sufficient de-bundling and dispersion of MWCNT in the nanocellulosic suspensions, while at the same time avoiding excessive damage to the MWCNT and nanocellulose structures.[44] The dispersions were stored in a refrigerator at ∼5 °C and have been found to be stable based on visual observations, over a period of 9 months at the time of writing of this manuscript (Figure 2a, photograph of the suspensions).

2.3. Physicochemical Characterization Methods. Elemental analysis was carried out using a FLASH 2000 series elemental analyzer (Thermo Scientific) on functionalized nanocellulosic materials dried in an oven at 60 °C overnight. Conductometric titration was performed according to the standard SCAN-CM 65:0278, as per the procedure described by Reyes et al.,[45] using an automatic titration device (Metrohm 751 GPD Titrino and Tiamo 1.2.1 software). ζ-Potentials were determined using a Zetasizer Nano-ZS90 (Malvern) instrument. Fourier transform infrared (FTIR) spectroscopy in attenuated total reflection (ATR) mode was carried out using a Bruker Alpha II FTIR spectrometer. UV−visible spectroscopy was carried out on 1000× diluted nanocellulose/MWCNT suspensions using a Shimadzu UV-2600 spectrophotometer (Shimadzu Corp., Kyoto, Japan) in the 200−800 nm wavelength range. Scanning electron microscopy (SEM) images were obtained using a Hitachi S-4700 scanning electron microscope. Transmission electron microscopy (TEM) images of the functionalized nanocellulosic materials were obtained using an FEI TALOS F200X FEG system, with an acceleration voltage of 200 kV. The corresponding nanocellulose/

https://doi.org/10.1021/acsanm.1c00774
ACS Appl. Nano Mater. 2021, 4, 5842−5853

Table 2. Summary of Physicochemical Properties of the Functionalized Nanocellulosic Materials and Drop-Cast Nanocellulose/MWCNT Membranes

nanocellulose	SCNF	TOCNF	SCNC	ACNC
charge density[a] (mmol/g)	1.7 [OSO_3^-]	1.3 [COO^-]	0.17 [OSO_3^-]	0.12 [OSO_3^-], 0.68 [NH_3^+]
ζ-potential[b] (mV)	−35.7 ± 0.5	−33.1 ± 0.1	−35 ± 1.4	−27.7 ± 2.4
width[c] (nm)	4.2 ± 1.1	2.9 ± 0.8	5.1 ± 1.7	4.0 ± 1.3
nanocellulose/MWCNT composite	SCNF/MWCNT	TOCNF/MWCNT	SCNC/MWCNT	ACNC/MWCNT
thickness[d] (μm)	2.27 ± 0.4	2.68 ± 0.3	1.82 ± 0.1	1.47 ± 0.2

[a]Measured from elemental analysis for SCNF, SCNC, ACNC, and conductometric titration for TOCNF. [b]Measured in 1 mM PBS solution (n = 3). [c]Estimated from TEM images (Figure 3e−h). Note: MWCNT dimensions as provided by the manufacturer: 30 ± 15 nm diameter, 5−20 μm length. [d]Profilometry measurements on pristine electrodes (n = 6).

MWCNT suspensions were imaged using a JEOL JEM-2800 high-throughput, high-resolution TEM system, with an acceleration voltage of 200 kV. Profilometry measurements were carried out using a Veeco Dektak 6M stylus profilometer, to estimate the overall thickness profiles of the drop-cast electrodes. Further details on sample preparation and measurement protocols for all physicochemical methods are provided in the Supporting Information.

2.4. Electrode Fabrication and Electrochemistry. The ta-C thin-film electrodes were prepared using pulsed filtered cathodic vacuum arc (p-FCVA) deposition. The preparation and characterization of these electrodes are described in detail in previous works.[32,46] In brief, a highly conductive p-type boron-doped ⟨100⟩ silicon wafer, with resistivity <0.005 Ω cm (Siegert Wafer, Germany), was first deposited with an ∼20 nm Ti adhesion layer by sputtering, followed by a 7 nm ta-C layer. The ta-C coated wafer was then diced into 5 × 5 mm^2 pieces using an automated dicing saw (DAD 3220, Disco). The pieces were individually packaged onto copper-clad FR4-PBB strips using poly(tetrafluoroethylene) (PTFE) tape (Saint-Gobain Performance Plastics CHR 2255-2), with a 3 mm diameter (0.07 cm^2) circular exposed electrode area. The exposed electrode area was functionalized with a polyethyleneimine (PEI) anchoring layer, by drop-casting 15 μL of 0.1 wt % PEI suspension, waiting for 10 min, and rinsing thoroughly in Milli-Q water. The electrodes were dried with gentle nitrogen flow and drop-cast with 7 μL of the nanocellulose/MWCNT suspensions, followed by drying for 1 h in an oven at 80 °C, under ambient pressure. A schematic of the nanocellulose/MWCNT composite electrode preparation is shown in Figure 2b, and optical microscope images of the pristine dried drop-cast electrodes are shown in Figure 2c.

Electrochemical properties of the nanocellulose/MWCNT composite electrodes were assessed using CV measurements with a Gamry Reference 600 potentiostat. A conventional three-electrode setup with a platinum counter wire and Ag/AgCl reference electrode (+0.199 V vs standard hydrogen electrode (SHE), Radiometer Analytical) was used. The analytes, $Ru(NH_3)_6Cl_3$ (hexaammineruthenium(III) chloride), and K_2IrCl_6 (potassium hexachloroiridate(IV)), were purchased from Sigma-Aldrich. Measurements were carried out in 10 mM phosphate buffer saline (PBS) solution (pH = 7.4) and 1 M KCl solution. The electrolytes were bubbled with nitrogen 20 min prior to measurements, and the electrochemical cell was kept at nitrogen overpressure during measurements to maintain an inert atmosphere, and all of the measurements were carried out at room temperature.

3. RESULTS AND DISCUSSION

3.1. Chemical and Physical Properties. *3.1.1. Charge Density.* Elemental sulfur and nitrogen contents (wt %) per gram of dry SCNF, SCNC, and ACNC nanocellulosic materials were estimated by elemental analysis. SCNF (prepared by direct sulfation using sulfamic acid and urea mixture) showed the highest elemental content of 5.44% S (≡ 1.7 mmol/g OSO_3^-), in addition to 2.76% elemental N (≡ 1.97 mmol/g NH_4^+) from the ammonium sulfate reaction product.[36] This degree of sulfate (OSO_3^-) group substitution in SCNF is comparable to the sulfonic group (SO_3^-) substitution of Nafion, a commonly used ion-exchange polymer, that is commercially available with 1.03−0.93 mmol/g of SO_3^- substitution. Sulfuric acid-hydrolyzed SCNC material showed a 10 times lower value of 0.55% S (≡ 0.17 mmol/g OSO_3^-). The ACNC material showed 0.38% S (≡ 0.12 mmol/g OSO_3^-) from the sulfated raw material (CelluForce NCC), as well as 0.95% N (≡ 0.68 mmol/g NH_3^+). The amount of carboxyl groups present in cellulosic materials cannot be unambiguously estimated from elemental analysis due to the carbon and oxygen present in the cellulose structure, and therefore conductometric titration is more widely used.[37,47] The degree of substitution of carboxyl groups in the TEMPO-oxidized pulp was estimated to be 1.3 mmol/g (COO^-) by conductometric titration as per standard SCAN-CM 65:0278 procedure. These results indicate that the fibrillar materials used in this work have a higher degree of functional group substitution compared to the crystalline materials.

3.1.2. ζ-Potential. The ζ-potential measurements were carried out in 0.1× PBS at pH 7.4, to mimic the electrochemical measurement environment (Figure S1, ζ-potential distributions). All suspensions show negative ζ-potential values below −27 mV (see Table 2), indicating the presence of predominantly negative charges on the nanocellulosic surfaces. It must be noted that the ζ-potential values were estimated using the Smoluchowski model in Zetasizer software (version 7.12), and the arbitrary fibrillar nanocellulosic geometries can therefore lead to higher artifacts in the measured values compared to crystalline materials.[48] Further, the higher valence ions present in PBS can also result in a lower ζ-potential value.[49] Therefore, the ζ-potential values for different functionalized nanocellulosic materials presented in Table 2 must be considered qualitatively.

3.1.3. ATR-FTIR. Infrared absorbance spectra (Figure S2) were obtained for functionalized nanocellulosic materials and composites, as well as reference MWCNT, in 400−4000 cm^{-1} range, with 4 cm^{-1} resolution and 32 scans per measurement. In the lower spectral range from 700 to 1800 cm^{-1}, the nanocellulosic materials show characteristics peaks corresponding to the stretching and bending vibrations of the cellulose backbone,[50] as well as some clear peaks corresponding to different functional groups (Table S1, peak associations). SCNF spectrum shows the highest intensity of sulfate functional group peaks corresponding to the symmetrical C−O−S stretching vibrations and asymmetrical S═O vibrations at 810 and 1250 cm^{-1}, respectively. In addition, NH_4^+ deformation vibrations from the ammonium sulfate salt[36] are observed as a broad shoulder on the SCNF spectrum, around 1470 cm^{-1}. The SCNC and ACNC spectra closely resemble each other, and amino-silane functional group-specific

https://doi.org/10.1021/acsanm.1c00774
ACS Appl. Nano Mater. 2021, 4, 5842−5853

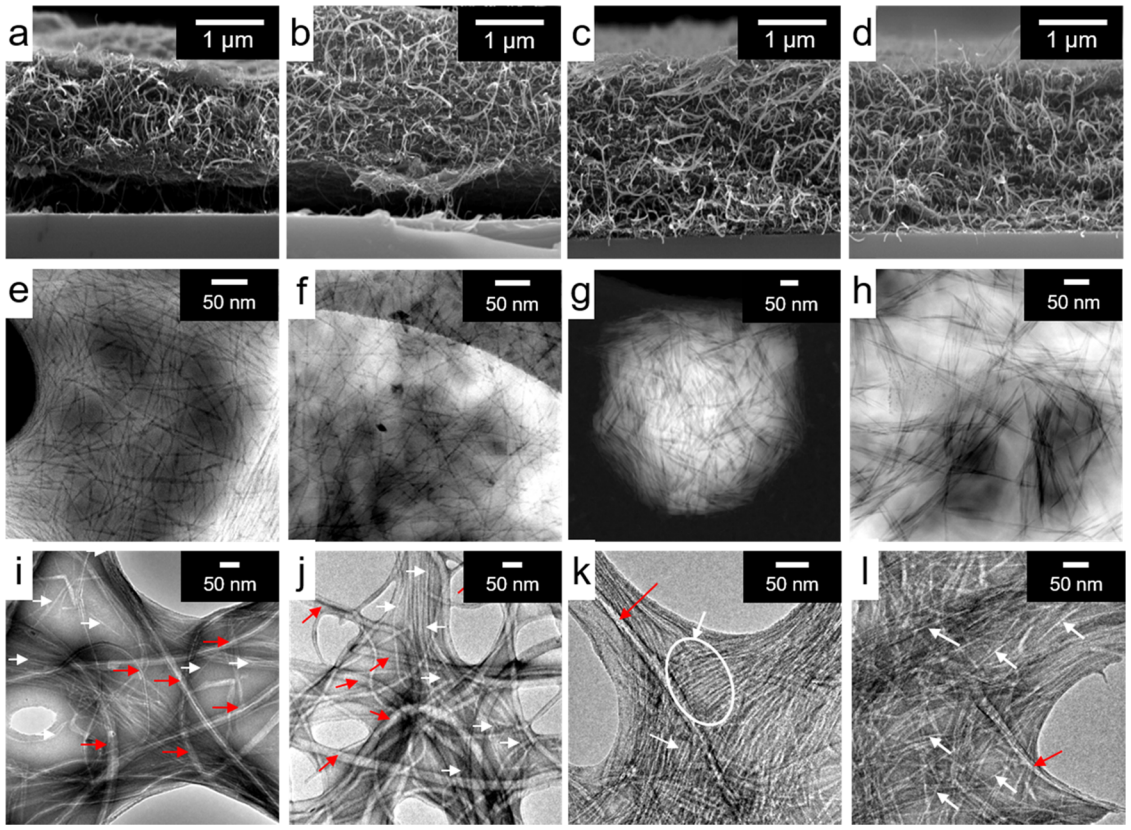

Figure 3. Cross-sectional SEM images of the drop-cast SCNF/MWCNT, TOCNF/MWCNT, SCNC/MWCNT, and ACNC/MWCNT electrodes (a–d, respectively). TEM images of pure SCNF, TOCNF, SCNC, and ACNC (e–h, respectively), and their corresponding composites with MWCNT (i–l, respectively). In the composite samples, nanocellulosic materials are marked by white arrows and MWCNTs are shown with red arrows.

vibrations could not be distinguished from the ACNC sample due to large interference from the sulfate groups and backbone vibrations of the cellulose molecules. The TOCNF spectrum shows strong carboxylic group (COO^-) stretching vibrations at ~1610 cm^{-1}, likely broadened due to the overlapping H–O–H stretching vibrations at ~1634 cm^{-1}.[51] Some of these nanocellulose and functional group-specific vibrations are also observed in the corresponding nanocellulose/MWCNT composite spectra as weak peaks masked by the large absorbance from MWCNT.

3.1.4. UV–Visible Spectroscopy. The UV–visible absorption spectra of 1000× diluted nanocellulose and the corresponding composite suspensions in the 200–800 nm wavelength range are shown in the Supporting Information (Figure S3). Pure nanocellulosic materials show almost negligible absorbance in this region, whereas all composite materials show a clear absorption peak at ~260 nm, corresponding to the MWCNT.[52,53] It has previously been reported in the literature that the intensity of the CNT absorption peak can be related to the dispersion or debundling of the CNTs, as bundled CNTs exhibit almost no absorbance in the UV–vis region due to the quenching, resulting from increased contact and carrier tunneling.[54,55] SCNF/MWCNT composite shows the highest absorption at ~260 nm, indicating that the fibrillar geometry, together with the high degree of sulfate functional groups, improves the dispersion of MWCNT in aqueous media. The absorption peak of the TOCNF/MWCNT composite is slightly broader than the other materials, possibly due to the absorption of C=O transitions in the carboxylic group ~240 nm, which is also observed in the TOCNF suspension.[56] ACNC/MWCNT shows the lowest absorbance.

3.1.5. SEM and TEM. Planar and cross-sectional morphologies of the drop-cast composite electrodes were investigated using scanning electron microscopy. The planar SEM images (Figure S4a–d) show a dense network of well-dispersed MWCNT over the entire electrode surface for all four types of composites. Cross-sectional SEM images (Figure 3a–d) show dense, well-dispersed MWCNT throughout the thickness of the film, with no apparent clustering or gradients in the distribution. The SEM samples in this work were prepared in a similar manner to the working electrodes, to assess the dispersion of MWCNT in the electrode structures, and are therefore not suitable for high-resolution imaging of the individual components. Although the nanocellulosic components cannot be unambiguously identified in these SEM images, the homogeneous distribution of MWCNT indicates efficient distribution of both components within the film.

Model films for TEM samples were prepared from 0.05 wt % pure nanocellulosic materials and 50× diluted nanocellulose/MWCNT suspensions, for better clarity of individual components. TEM images of the pure SCNF and TOCNF suspensions (Figure 3e,f, respectively) show homogeneous distribution of individual fibers, with widths of 4.2 ± 1.1 and 2.9 ± 0.8 nm, respectively, and SCNC and ACNC materials (Figure 3g,h, respectively) show uniform rodlike structures, with widths in the range of 5.1 ± 1.7 and 4.0 ± 1.3 nm, respectively. Based on the literature, the lengths of fibrillar

https://doi.org/10.1021/acsanm.1c00774
ACS Appl. Nano Mater. 2021, 4, 5842–5853

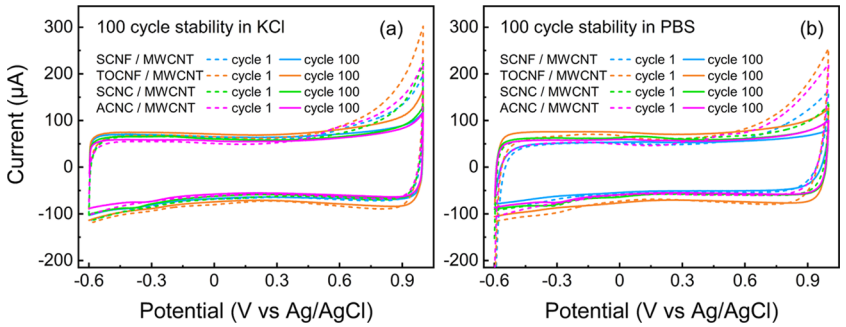

Figure 4. Background currents from CV cycles 1 (dashed line) and 100 (solid line), for different nanocellulose/MWCNT composite electrodes, in blank 1 M KCl (a) and 10 mM PBS (b), at a 500 mV/s scan rate.

nanocellulosic materials are expected to be in the range of few microns,[57] whereas the lengths of crystalline nanocellulosic materials are typically much lower, in the order of 100−120 nm for cotton-based material[58] (SCNC in this work), and <100 nm for wood-based material[59] (ACNC in this work). This is clearly observed in the corresponding nanocellulose/MWCNT composite TEM images (Figure 3i−l) showing fibrillar and crystalline nanocellulosic material (white arrows) surrounding hollow multiwalled carbon nanotubes (red arrows). The long fibrillar materials (SCNF and TOCNF, Figure 3i,j, respectively) can be seen both as thin individual fibrils and bundles, interspersed with the hollow MWCNT. The short crystalline structures (SCNC and ACNC, Figure 3k,l, respectively) appear more densely packed around the MWCNT. Additional low- and high-magnification TEM images are presented in the Supporting Information (Figure S5).

3.1.6. Profilometry. Overall thickness profiles of the drop-cast nanocellulose/MWCNT membranes on top of ta-C were examined using a stylus profilometer. All samples showed two distinct thickness regimes (Figure S6), with an outer (~800 μm wide) ring showing higher thickness, compared to the central region. This fringe pattern is a typical artifact observed in drop-cast films due to the gradient in solvent evaporation, and is referred to as the coffee-ring effect.[60] This coffee-ring effect is observed to be most pronounced for the ACNC/MWCNT composite, as seen from both optical microscope images (Figure 2c) and profilometry measurements (Figure S6). This can be attributed to the large dimensional mismatch between the ACNC and MWCNT, resulting in higher surface tensions and thereby pronounced pitting formation of these films during drying.[61] The average thicknesses of the different drop-cast membranes were estimated from the central ~1.5 mm diameter region, and the values are tabulated in Table 2 (n = 6). Fibrillar nanocellulosic composites are thicker compared to crystalline nanocellulosic composites, supporting the formation of denser architectures for crystalline nanocellulosic composites, as observed also in TEM images. The physicochemical characterization results are summarized in Table 2.

3.2. Electrochemical Behavior. Electrochemical performance of the nanocellulose/MWCNT composite membranes, drop-cast on ta-C electrodes, was investigated using CV measurements in 1 M KCl and 10 mM PBS. A standard 10 mM PBS solution contains 137 mM NaCl, 2.7 mM KCl, 10 mM Na_2HPO_4, and 1.8 mM KH_2PO_4. These ionic concentrations are similar to those of physiological fluids, and hence PBS is often used as an electrolyte in biosensor research.

3.2.1. Electrode Stability. To ensure a stable hydrated state, all electrodes were presoaked in the respective measurement electrolytes for 45 min prior to the measurements and kept immersed during the entire duration of measurements (~7 h). All electrodes were found to be highly stable in the chosen electrolyte solutions over this time period, with no delamination. Profilometry measurements of pristine electrodes as well as "used" electrodes after 7 h immersion in PBS/KCl are shown in Figure S6. The average thickness values of the used electrodes remain in the same range as that of the pristine electrodes, within the standard deviations (Table 2). The introduction of PEI on the hydrophobic ta-C surface is thus considered to be successful in anchoring the drop-cast nanocellulose/MWCNT membranes, without the need for any additional polymeric binders in the composite, as previously used.[23] Electrochemical measurements in blank electrolyte solutions further verify that the introduction of PEI does not passivate the ta-C substrate (Figure S7). Structural stabilities of the drop-cast electrode membranes were also investigated in deionized water. The SCNF/MWCNT composite was found to rapidly delaminate from the ta-C substrate and redisperse in deionized water (Figure S8). However, this behavior was not observed for the other three types of nanocellulose/MWCNT membranes. The high degree of sulfation (1.7 mmol/g) of the SCNF likely causes pronounced electrostatic repulsion in deionized water with less than 1 ppb ions, resulting in the SCNF/MWCNT membrane instability.[62] In contrast, screening of some of these nanocellulosic surface charges by the salts present in the electrolyte media (e.g., 10 mM PBS = ionic strength 167 mM) prevents the redispersion of SCNF/MWCNT during electrochemical measurements in this study.

3.2.2. Background Currents. All electrodes were first cycled in the blank measurement electrolyte (PBS or KCl) for at least 25 cycles, at a scan rate of 500 mV/s, before measuring any analyte. This protocol was to ensure the electrode quality and establish stable background current. Some faradic peaks and slightly higher anodic currents were observed (above +0.6 V) in the first cycle, possibly due to the oxidation of impurities on the MWCNT. However, the background currents of all composites stabilized over the entire potential range with consecutive cycling, and no changes were observed after the 25th cycle (Figure S9, cycles 1, 25, 50, and 75). Background CV cycles 1 and 100 of different nanocellulose/MWCNT composites are shown over a potential range of −0.6 to +1 V vs Ag/AgCl reference electrode, in Figure 4a,b, for 1 M KCl and 10 mM PBS, respectively.

https://doi.org/10.1021/acsanm.1c00774
ACS Appl. Nano Mater. 2021, 4, 5842−5853

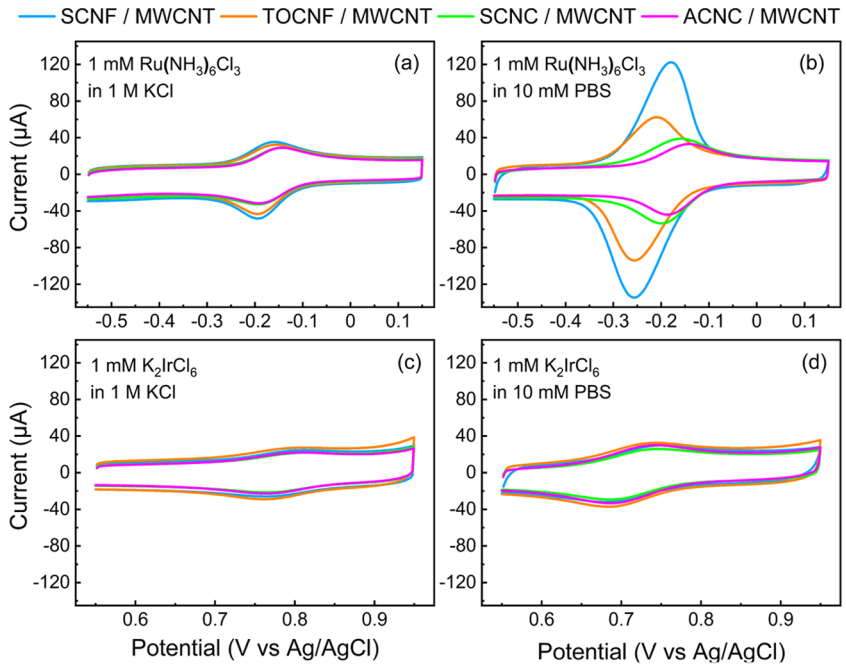

Figure 5. Cyclic voltammograms of different nanocellulose/MWCNT composite electrodes, for 1 mM $Ru(NH_3)_6Cl_3$ in 1 M KCl (a) and 10 mM PBS (b), and 1 mM K_2IrCl_6 in 1 M KCl (c) and 10 mM PBS (d), respectively, at a 100 mV/s scan rate.

From the CVs in blank electrolytes at different scan rates (50 to 500 mV/s, Figures S10 and S11, in KCl and PBS, respectively), pseudocapacitance per geometrical electrode area[63] (0.07 cm^2) was calculated for different composite electrode types according to the equation $C = (I_a - I_c)/(2 \times \text{scan rate})$, where I_a and I_c are the anodic and cathodic currents averaged over three potential ranges (−0.15 to −0.05, 0.2 to 0.3, and 0.45 to 0.55 V), respectively. Average pseudocapacitance values are given in Table S2, for both KCl and PBS. In both electrolytes, all composite electrodes showed a 100-fold increase in geometrical pseudocapacitance (>1.5 mF/cm^2) compared to that of the ta-C substrate (∼10 μF/cm^2). These values are over 5 times higher than the geometrical pseudocapacitance of 349 ± 87 μF/cm^2 observed by Sainio et al.,[64] for MWCNT grown on diamond-like carbon thin films by catalytic vapor deposition. Water window of the composites was tested in 0.15 M H_2SO_4 (Figure S12), with 1 mA threshold current, at 400 mV/s scan rate. All composites showed a wide potential window (∼2.6 V), with the oxygen evolution reaction (OER) occurring at +1.6 V and the hydrogen evolution reaction (HER) occurring at −1 V. The stable wide potential window and large geometrical pseudocapacitance indicate good potential for energy storage applications.

3.2.3. Outer-Sphere Redox Probes Sensing. CVs of 1 mM $Ru(NH_3)_6Cl_3$ measured with the four different nanocellulose/MWCNT composite electrodes, in 1 M KCl and 10 mM PBS, at a 100 mV/s scan rate, are shown in Figure 5a,b, respectively.

In 1 M KCl, the fibrillar nanocellulose/MWCNT composites behave very similarly to each other, with peak separations (ΔE_p) of 35.9 and 39.9 mV, for SCNF/MWCNT and TOCNF/MWCNT, respectively. The two crystalline nanocellulose/MWCNT matrices resemble each other, with slightly larger ΔE_p values of 49.9 and 48.3 mV for SCNC/MWCNT and ACNC/MWCNT, respectively. Redox currents (baseline-subtracted I_{pa}, I_{pc}) for all composites (see Table S2) are of similar magnitude (∼20 μA) in 1 M KCl. However, in 10 mM PBS (Figure 5b), large differences are observed between the different composites, in both peak current and ΔE_p values. The SCNF/MWCNT composite has a ΔE_p of 74.6 mV and significantly higher redox currents (I_{pa} = 107.6 μA, I_{pc} = −119.2 μA), compared to other composites. The TOCNF/MWCNT composite also shows a relative increase in ΔE_p (48.6 mV) and a nonsymmetrical increase in the redox currents (I_{pa} = 49.4 μA, I_{pc} = 80.9 μA) in PBS compared to KCl.

In contrast, the crystalline composites show only a slight decrease in ΔE_p and almost same redox currents (∼20 μA), in PBS compared to KCl. The formal potential of the $Ru(NH_3)_6^{2+/3+}$ redox couple shows a negative (cathodic) shift in PBS for all of the composites, compared to 1 M KCl. The ratio of I_{pa}/I_{pc} is less than unity (<1) for all composites, indicating that the more positively charged oxidation product $Ru(NH_3)_6^{3+}$ is more strongly electrostatically adsorbed in the negatively charged nanocellulose/MWCNT matrices. CVs for 1 mM K_2IrCl_6 in 1 M KCl and 10 mM PBS are shown in Figure 5c,d, respectively, at a 100 mV/s scan rate. Redox currents for the $IrCl_6^{4-/3-}$ system are approximately half (∼10 μA) that of the $Ru(NH_3)_6^{2+/3+}$ system, in both KCl and PBS. Further, no composite-specific increase in currents is observed in PBS for $IrCl_6^{4-/3-}$, as is observed for $Ru(NH_3)_6^{2+/3+}$. However, the formal potential of $IrCl_6^{4-/3-}$ redox couple also shows a negative (cathodic) shift in PBS for all of the composites, compared to 1 M KCl.

Both $Ru(NH_3)_6^{2+/3+}$ and $IrCl_6^{4-/3-}$ redox couples are surrounded by a strong hydration shell that inhibits their specific adsorption, and are therefore insensitive to surface functional groups. The results obtained in this study can therefore be predominantly attributed to electrostatic effects, due to the charged functional groups present on the nanocellulosic materials in the composite electrodes. Similar trends in the behavior of $Ru(NH_3)_6^{2+/3+}$ redox couple have been observed in ion-exchange membranes such as Nafion, in electrolytes of varying ionic compositions and concentra-

https://doi.org/10.1021/acsanm.1c00774
ACS Appl. Nano Mater. 2021, 4, 5842−5853

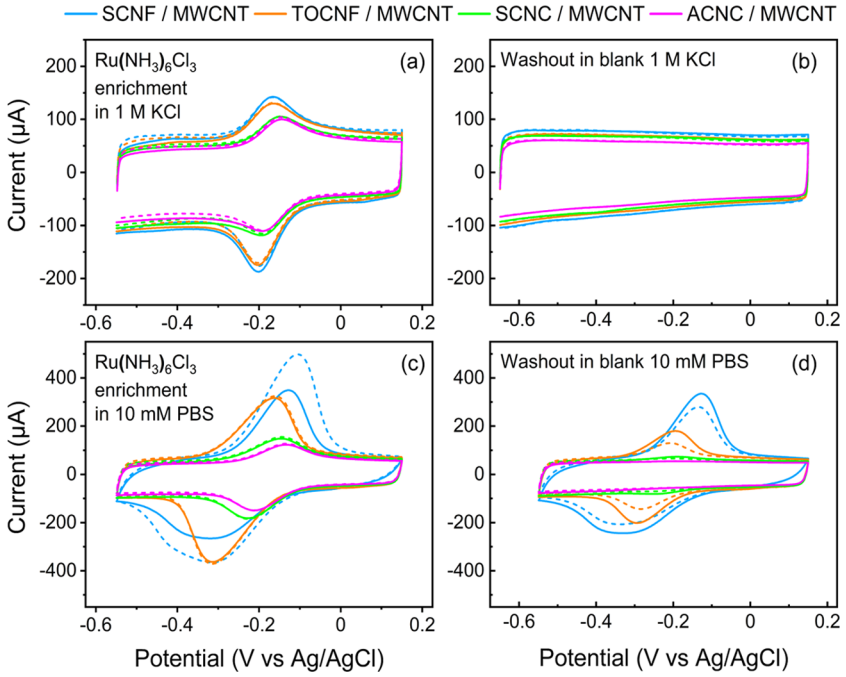

Figure 6. Cyclic voltammograms of different nanocellulose/MWCNT composite electrodes at a 500 mV/s scan rate, showing 1st (solid line) and 25th (dashed line) cycles, for enrichment and washout measurements in 1 M KCl (a, b) and 10 mM PBS (c, d), respectively.

tions.[65] Shi et al.[66] demonstrated that the movement of $Ru(NH_3)_6^{2+/3+}$ ions in Nafion membrane is dominated by their physical motion along the pathways dictated by the sulfonic groups, and the oxidation product $Ru(NH_3)_6^{3+}$ is more strongly bound in the membrane due to stronger electrostatic interactions. Further, an investigation by Thielemans et al.,[67] on sulfuric acid-hydrolyzed cellulose nanowhiskers as ion-exchange membranes, in a 0.1 M KCl electrolyte, indicated that the $Ru(NH_3)_6^{3+}$ ions were strongly electrostatically bound in the cellulose membrane.

3.2.4. Enrichment and Washout of $Ru(NH_3)_6^{2+/3+}$. The significantly higher redox currents for cationic $Ru(NH_3)_6^{2+/3+}$ redox couple in 10 mM PBS, compared to 1 M KCl, specifically in the fibrillar nanocellulosic matrices (SCNF and TOCNF), indicate a stronger enrichment of the cationic redox probe in the predominantly anionic nanocellulose/MWCNT composites. Although the crystalline nanocellulosic materials (SCNC and ACNC) are also predominantly negatively charged (see Table 2 for charge density and ζ-potential results), the $Ru(NH_3)_6^{2+/3+}$ redox current increase in lower ionic strength is much less pronounced for the crystalline composites. This effect is further studied by carrying out enrichment and washout studies at the different nanocellulose/MWCNT composite platforms. The composite electrodes were first scanned for 25 cycles in a 1 mM $Ru(NH_3)_6$ solution in different electrolytes, followed by a 20 min washout in the respective blank electrolytes. After washout, the electrodes were again scanned for 25 cycles in the blank electrolyte solutions. The 1st- and 25th-cycle CVs for $Ru(NH_3)_6$ enrichment and washout measurements in both 1 M KCl and 10 mM PBS are shown in Figure 6.

In 1 M KCl, all electrodes show relatively steady redox currents for 25 cycles scan in 1 mM $Ru(NH_3)_6$ solution (Figure 6a), with no apparent enrichment, and the post-washout scans in blank 1 M KCl show no discernible redox peaks even in the first cycle, indicating no residual $Ru(NH_3)_6$ in the composites after the measurement in 1 M KCl (Figure 6b). However, in 10 mM PBS (Figure 6c), the 25 cycle enrichment in 1 mM $Ru(NH_3)_6$ solution shows a clear (1.5 times) increase in the redox currents from the 1st cycle to the 25th cycle for the SCNF/MWCNT composite. This effect was negligible in other composite types. Post-washout measurements in blank 10 mM PBS further confirmed the strong electrostatic binding of the $Ru(NH_3)_6^{2+/3+}$ ions inside the SCNF/MWCNT composite membrane, where clear redox peaks are observed even after 25 cycles in the blank electrolyte (Figure 6d). The TOCNF/MWCNT composite also shows strong redox peaks after washout, however, to a lesser extent compared to the SCNF/MWCNT matrix. A small residual peak is observed also in the SCNC/MWCNT matrix, but is not discernible in the ACNC/MWCNT matrix. The electrostatic effects were also verified in 0.1 M KCl, with ionic strength in the same order of magnitude as that of 10 mM PBS, and a similar trend was also observed in this case (Figure S13). Thus, the SCNF/MWCNT membrane, with the highest amount (1.7 mmol/g) of sulfate groups, shows the strongest electrostatic enrichment of cationic $Ru(NH_3)_6^{2+/3+}$, followed by the TOCNF/MWCNT membrane, with 1.3 mmol/g carboxylic group substitution.

In addition to the nanocellulosic functionalization-dependent electrostatic effects, the effects of nanocellulose geometry on the morphology of the corresponding composite membranes in the swollen state must also be taken into account. Although there are no direct characterization techniques to estimate the swollen state porosity of the micron-thick composites in the different electrolytes, it can be hypothesized from the TEM images and profilometry measurements (Table 2) that the fibrillar nanocellulosic materials form a more porous network with the MWCNT, while the crystalline nanocellulosic materials form denser composite architectures. The literature on nanocellulosic thin films (nm thickness) indicates that highly charged TEMPO-oxidized cellulose

https://doi.org/10.1021/acsanm.1c00774
ACS Appl. Nano Mater. 2021, 4, 5842−5853

nanofibrillar films show a nearly 4-fold increase in thickness (from 13 to 50 nm) with a 97% increase in relative humidity (RH),[68] whereas crystalline nanocellulose films show only 0.25 times increase in thickness for a similar increase in RH.[69] Further, the ionic strength of the medium has also been shown to influence the hydration and swelling of charged nanocellulosic films.[70] These findings further support the hypothesis that the fibrillar nanocellulosic composites likely exhibit higher swelling than the crystalline nanocellulosic composites, thereby having larger pores in the swollen state.

Thus, the strong residual $Ru(NH_3)_6^{2+/3+}$ peaks observed in PBS for the fibrillar nanocellulosic composites (Figure 6d) can be explained as a combination of (i) electrostatic interactions with the higher density of negative surface functional groups and (ii) physical entrapment of molecules within the more porous structures. This effect is more pronounced in the lower-ionic-strength electrolyte (10 mM PBS compared to 1 M KCl), due to lesser screening of the negative charges on fibrillar nanocellulosic surfaces, and consequently stronger electrostatic effects and also higher swelling of the fibrillar matrices.[70] In contrast, the crystalline nanocellulose/MWCNT composites, with a lower degree of anionic group substitution and denser architectures, show negligible residual peaks for the $Ru(NH_3)_6^{2+/3+}$ redox couple, indicating both weaker electrostatic interactions and absence of physical entrapment. The anionic $IrCl_6^{4-/3-}$ redox couple shows neither electrostatic nor physical enrichment in any of the studied composites, indicating that the predominantly negative functional groups on the nanocellulose materials result in strong electrostatic repulsion, which largely prevents the enrichment of the anionic molecules even within the more porous nanofibrillar matrices.

Based on these results, some general design guidelines for developing nanocellulose/MWCNT-based electrochemical platforms can be surmised as follows: (i) morphological selectivity can be tailored by changing the nanocellulosic material dimensions, where the use of fibrillar nanocellulosic materials can result in more porous structures suitable for physical enrichment of analyte molecules; (ii) ionic selectivity can be tailored by changing the nature and degree of functional group substitution on the nanocellulosic materials, where a high density of more negative functional group results in strong electrostatic effects; and (iii) differential screening of nanocellulosic surface charges, by varying the ionic strength of the supporting electrolyte, can offer tunable electrochemical performance of such composites. These insights can help develop optimized nanocellulose/carbon nanomaterial-based platforms for various electrochemical applications, simply by tailoring the nanocellulosic component properties.

4. CONCLUSIONS

To summarize, in this study, we have (i) produced four different nanocellulosic materials, with different geometries and surface functionalizations, (ii) shown that all of these different nanocellulosic materials are capable of forming stable aqueous dispersions of commercial MWCNT without the need for economically or environmentally taxing pretreatments and additives, and (iii) demonstrated that these suspensions can be used to produce highly stable and repeatable electrochemical platforms by a robust drop-casting method. Electrochemical characterizations of all four nanocellulose/MWCNT composites showed excellent stability in different electrolyte solutions, over a wide potential range (−0.6 to +1 V), indicating their suitability for different electrochemical applications. In a 1 M KCl electrolyte, the electrochemical behaviors of OSR probes at all composites were similar, indicating that both fibrillar and crystalline nanocelluloses are capable of producing stable, high-surface-area networks of MWCNT suitable for electrochemical applications. In a physiologically relevant, lower-ionic-strength electrolyte (10 mM PBS), the interrelated differences in density (and type) of functionalization and geometry of the nanocellulosic materials showed a strong influence on both physical and electrostatic interactions of the OSR probes at the corresponding composite membranes. To the best of the authors' knowledge, this study is the first attempt to characterize the electrochemical performance of such nanocellulose/MWCNT composite platforms in electrolytes of different ionic strengths and correlate them to the differences in the constituent nanocellulosic material geometry and functionalization. The insights from this study offer a promising route to design highly selective, environmentally friendly, and industrially scalable electroanalytical platforms for biosensing and environmental monitoring applications.

■ ASSOCIATED CONTENT

Supporting Information

The Supporting Information is available free of charge at https://pubs.acs.org/doi/10.1021/acsanm.1c00774.

Details of ζ-potential measurement protocol and distributions; ATR-FTIR sample preparation and absorbance spectra with peak associations; UV−visible spectroscopy sample preparation and absorbance spectra; SEM and TEM sample preparation and additional images; profilometry sample preparation and results; effect of PEI functionalization on ta-C electrochemical performance; effect of deionized water on different electrodes; cycling performance of all composite electrodes; background CVs of all composite electrodes at different scan rates, in 1 M KCl and 10 mM PBS; water window in 0.15 M H_2SO_4; summary of electrochemical results of all composite electrodes; and washout of $Ru(NH_3)_6^{2+/3+}$ in 0.1 M KCl (PDF)

■ AUTHOR INFORMATION

Corresponding Author

Vasuki Durairaj − *Department of Chemistry and Materials Science, School of Chemical Technology, Aalto University, 00076 Aalto, Finland;* orcid.org/0000-0001-9632-1703; Phone: +358505138355; Email: vasuki.durairaj@aalto.fi

Authors

Panpan Li − *VTT Technical Research Centre of Finland, Solutions for Natural Resources and Environment, FI-02044 VTT, Finland*

Touko Liljeström − *Department of Chemistry and Materials Science, School of Chemical Technology, Aalto University, 00076 Aalto, Finland*

Niklas Wester − *Department of Chemistry and Materials Science, School of Chemical Technology, Aalto University, 00076 Aalto, Finland;* orcid.org/0000-0002-7937-9011

Jarkko Etula − *Department of Chemistry and Materials Science, School of Chemical Technology, Aalto University, 00076 Aalto, Finland;* orcid.org/0000-0002-6930-1165

Ilona Leppänen − *VTT Technical Research Centre of Finland, Solutions for Natural Resources and Environment, FI-02044 VTT, Finland*

https://doi.org/10.1021/acsanm.1c00774
ACS Appl. Nano Mater. 2021, 4, 5842−5853

Yanling Ge − *VTT Technical Research Centre of Finland, Solutions for Natural Resources and Environment, FI-02044 VTT, Finland*

Katri S. Kontturi − *VTT Technical Research Centre of Finland, Solutions for Natural Resources and Environment, FI-02044 VTT, Finland*

Tekla Tammelin − *VTT Technical Research Centre of Finland, Solutions for Natural Resources and Environment, FI-02044 VTT, Finland;* orcid.org/0000-0002-3248-1801

Tomi Laurila − *Department of Electrical Engineering and Automation, School of Electrical Engineering, Aalto University, 00076 Aalto, Finland;* orcid.org/0000-0002-1252-8764

Jari Koskinen − *Department of Chemistry and Materials Science, School of Chemical Technology, Aalto University, 00076 Aalto, Finland*

Complete contact information is available at: https://pubs.acs.org/10.1021/acsanm.1c00774

Notes

The authors declare no competing financial interest.

■ ACKNOWLEDGMENTS

This work was a part of the Academy of Finland's Flagship Programme under projects nos. 318890 and 318891 (Competence Center for Materials Bioeconomy, FinnCERES). The authors acknowledge the provision of facilities by Aalto University Bioeconomy and OtaNano−Nanomicroscopy Center (Aalto-NMC) and RawMatters research infrastructure (RAMI).

■ REFERENCES

(1) Tatsumi, H. The Dawn of Electrochemistry. *Rev. Polarogr.* **2000**, *46*, 3−7.

(2) Power, A. C.; Morrin, A. Electroanalytical Sensor Technology. In *Electrochemistry*; InTech: Rijeka, 2013; pp 141−178.

(3) Yang, C.; Denno, M. E.; Pyakurel, P.; Venton, B. J. Recent Trends in Carbon Nanomaterial-Based Electrochemical Sensors for Biomolecules: A Review. *Anal. Chim. Acta* **2015**, *887*, 17−37.

(4) Sanghavi, B. J.; Wolfbeis, O. S.; Hirsch, T.; Swami, N. S. Nanomaterial-Based Electrochemical Sensing of Neurological Drugs and Neurotransmitters. *Microchim. Acta* **2015**, *182*, 1−41.

(5) Power, A. C.; Gorey, B.; Chandra, S.; Chapman, J. Carbon Nanomaterials and Their Application to Electrochemical Sensors: A Review. *Nanotechnol. Rev.* **2018**, *7*, 19−41.

(6) Osorio, A. G.; Silveira, I. C. L.; Bueno, V. L.; Bergmann, C. P. H2SO4/HNO3/HCl-Functionalization and Its Effect on Dispersion of Carbon Nanotubes in Aqueous Media. *Appl. Surf. Sci.* **2008**, *255*, 2485−2489.

(7) Vaisman, L.; Wagner, H. D.; Marom, G. The Role of Surfactants in Dispersion of Carbon Nanotubes. *Adv. Colloid Interface Sci.* **2006**, *128*−*130*, 37−46.

(8) Ausman, K. D.; Piner, R.; Lourie, O.; Ruoff, R. S.; Korobov, M. Organic Solvent Dispersions of Single-Walled Carbon Nanotubes: Toward Solutions of Pristine Nanotubes. *J. Phys. Chem. B* **2000**, *104*, 8911−8915.

(9) Lee, J. H.; Paik, U.; Choi, J. Y.; Kim, K. K.; Yoon, S. M.; Lee, J.; Kim, B. K.; Kim, J. M.; Park, M. H.; Yang, C. W.; An, K. H.; Lee, Y. H. Dispersion Stability of Single-Walled Carbon Nanotubes Using Nafion in Bisolvent. *J. Phys. Chem. C* **2007**, *111*, 2477−2483.

(10) Liu, Y.; Yu, L.; Zhang, S.; Yuan, J.; Shi, L.; Zheng, L. Dispersion of Multiwalled Carbon Nanotubes by Ionic Liquid-Type Gemini Imidazolium Surfactants in Aqueous Solution. *Colloids Surf., A* **2010**, *359*, 66−70.

(11) Olivier, C.; Moreau, C.; Bertoncini, P.; Bizot, H.; Chauvet, O.; Cathala, B. Cellulose Nanocrystal-Assisted Dispersion of Luminescent Single-Walled Carbon Nanotubes for Layer-by-Layer Assembled Hybrid Thin Films. *Langmuir* **2012**, *28*, 12463−12471.

(12) Lu, P.; Hsieh, Y. L. Preparation and Properties of Cellulose Nanocrystals: Rods, Spheres, and Network. *Carbohydr. Polym.* **2010**, *82*, 329−336.

(13) Jiang, F.; Hsieh, Y. L. Chemically and Mechanically Isolated Nanocellulose and Their Self-Assembled Structures. *Carbohydr. Polym.* **2013**, *95*, 32−40.

(14) Eyley, S.; Thielemans, W. Surface Modification of Cellulose Nanocrystals. *Nanoscale* **2014**, *6*, 7764−7779.

(15) Hajian, A.; Lindström, S. B.; Pettersson, T.; Hamedi, M. M.; Wågberg, L. Understanding the Dispersive Action of Nanocellulose for Carbon Nanomaterials. *Nano Lett.* **2017**, *17*, 1439−1447.

(16) Du, X.; Zhang, Z.; Liu, W.; Deng, Y. Nanocellulose-Based Conductive Materials and Their Emerging Applications in Energy Devices - A Review. *Nano Energy* **2017**, *35*, 299−320.

(17) Koga, H.; Saito, T.; Kitaoka, T.; Nogi, M.; Suganuma, K.; Isogai, A. Transparent, Conductive, and Printable Composites Consisting of TEMPO-Oxidized Nanocellulose and Carbon Nanotube. *Biomacromolecules* **2013**, *14*, 1160−1165.

(18) Yu, Z.; Hu, C.; Dichiara, A. B.; Jiang, W.; Gu, J. Cellulose Nanofibril/Carbon Nanomaterial Hybrid Aerogels for Adsorption Removal of Cationic and Anionic Organic Dyes. *Nanomaterials* **2020**, *10*, 1−19.

(19) Bacakova, L.; Pajorova, J.; Tomkova, M.; Matejka, R.; Broz, A.; Stepanovska, J.; Prazak, S.; Skogberg, A.; Siljander, S.; Kallio, P. Applications of Nanocellulose/Nanocarbon Composites: Focus on Biotechnology and Medicine. *Nanomaterials* **2020**, *10*, 1−32.

(20) Nguyen, H. K.; Bae, J.; Hur, J.; Park, S. J.; Park, M. S.; Kim, I. T. Tailoring of Aqueous-Based Carbon Nanotube − Nanocellulose Films as Self-Standing Flexible Anodes for Lithium-Ion Storage. *Nanomaterials* **2019**, *9*, No. 655.

(21) Wang, H.; Biswas, S. K.; Zhu, S.; Lu, Y.; Yue, Y.; Han, J.; Xu, X.; Wu, Q.; Xiao, H. Self-Healable Electro-Conductive Hydrogels Based on Core-Shell Structured Nanocellulose/Carbon Nanotubes Hybrids for Use as Flexible Supercapacitors. *Nanomaterials* **2020**, *10*, 1−21.

(22) Chen, W.; Yu, H.; Lee, S. Y.; Wei, T.; Li, J.; Fan, Z. Nanocellulose: A Promising Nanomaterial for Advanced Electrochemical Energy Storage. *Chem. Soc. Rev.* **2018**, *47*, 2837−2872.

(23) Durairaj, V.; Wester, N.; Etula, J.; Laurila, T.; Lehtonen, J.; Rojas, O. J.; Pahimanolis, N.; Koskinen, J. Multiwalled Carbon Nanotubes/Nanofibrillar Cellulose/Nafion Composite-Modified Tetrahedral Amorphous Carbon Electrodes for Selective Dopamine Detection. *J. Phys. Chem. C* **2019**, *123*, 24826−24836.

(24) Lu, S.; Bai, L.; Wen, Y.; Li, M.; Yan, D.; Zhang, R.; Chen, K. Water-Dispersed Carboxymethyl Cellulose-Montmorillonite-Single Walled Carbon Nanotube Composite with Enhanced Sensing Performance for Simultaneous Voltammetric Determination of Two Trace Phytohormones. *J. Solid State Electrochem.* **2015**, *19*, 2023−2037.

(25) Zhang, J.; Jiang, G.; Goledzinowski, M.; Comeau, F. J. E.; Li, K.; Cumberland, T.; Lenos, J.; Xu, P.; Li, M.; Yu, A.; Chen, Z. Green Solid Electrolyte with Cofunctionalized Nanocellulose/Graphene Oxide Interpenetrating Network for Electrochemical Gas Sensors. *Small Methods* **2017**, *1*, No. 1700237.

(26) Shahrokhian, S.; Naderi, L.; Ghalkhani, M. Nanocellulose/Carbon Nanoparticles Nanocomposite Film Modified Electrode for Durable and Sensitive Electrochemical Determination of Metoclopramide. *Electroanalysis* **2015**, *27*, 2637−2644.

(27) Ortolani, T. S.; Pereira, T. S.; Assumpção, M. H. M. T.; Vicentini, F. C.; Gabriel de Oliveira, G.; Janegitz, B. C. Electrochemical Sensing of Purines Guanine and Adenine Using Single-Walled Carbon Nanohorns and Nanocellulose. *Electrochim. Acta* **2019**, *298*, 893−900.

(28) Anirudhan, T. S.; Deepa, J. R.; Binussreejayan. Electrochemical Sensing of Cholesterol by Molecularly Imprinted Polymer of Silylated

Graphene Oxide and Chemically Modified Nanocellulose Polymer. *Mater. Sci. Eng., C* **2018**, *92*, 942−956.
(29) Shalauddin, M.; Akhter, S.; Basirun, W. J.; Bagheri, S.; Anuar, N. S.; Johan, M. R. Hybrid Nanocellulose/f-MWCNTs Nanocomposite for the Electrochemical Sensing of Diclofenac Sodium in Pharmaceutical Drugs and Biological Fluids. *Electrochim. Acta* **2019**, *304*, 323−333.
(30) Zhao, D.; Zhu, Y.; Cheng, W.; Chen, W.; Wu, Y.; Yu, H. Cellulose-Based Flexible Functional Materials for Emerging Intelligent Electronics. *Adv. Mater.* **2020**, No. 2000619.
(31) Xu, S.; Flynn, D.; Tay, B. K.; Prawer, S.; Nugent, K. W.; Silva, S. R. P.; Lifshitz, Y.; Milne, W. I. Mechanical Properties and Raman Spectra of Tetrahedral Amorphous Carbon Films with High Sp3 Fraction Deposited Using a Filtered Cathodic Arc. *Philos. Mag. B* **1997**, *76*, 351−361.
(32) Laurila, T.; Protopopova, V.; Rhode, S.; Sainio, S.; Palomäki, T.; Moram, M.; Feliu, J. M.; Koskinen, J. New Electrochemically Improved Tetrahedral Amorphous Carbon Films for Biological Applications. *Diamond Relat. Mater.* **2014**, *49*, 62−71.
(33) Peltola, E.; Wester, N.; Holt, K. B.; Johansson, L. S.; Koskinen, J.; Myllymäki, V.; Laurila, T. Nanodiamonds on Tetrahedral Amorphous Carbon Significantly Enhance Dopamine Detection and Cell Viability. *Biosens. Bioelectron.* **2017**, *88*, 273−282.
(34) Wester, N.; Sainio, S.; Palomäki, T.; Nordlund, D.; Singh, V. K.; Johansson, L. S.; Koskinen, J.; Laurila, T. Partially Reduced Graphene Oxide Modified Tetrahedral Amorphous Carbon Thin-Film Electrodes as a Platform for Nanomolar Detection of Dopamine. *J. Phys. Chem. C* **2017**, *121*, 8153−8164.
(35) Laurila, T.; Sainio, S.; Caro, M. Hybrid Carbon Based Nanomaterials for Electrochemical Detection of Biomolecules. *Prog. Mater. Sci.* **2017**, *88*, 499−594.
(36) Sirviö, J. A.; Ukkola, J.; Liimatainen, H. Direct Sulfation of Cellulose Fibers Using a Reactive Deep Eutectic Solvent to Produce Highly Charged Cellulose Nanofibers. *Cellulose* **2019**, *26*, 2303−2316.
(37) Saito, T.; Kimura, S.; Nishiyama, Y.; Isogai, A. Cellulose Nanofibers Prepared by TEMPO-Mediated Oxidation of Native Cellulose. *Biomacromolecules* **2007**, *8*, 2485−2491.
(38) Dong, X. M.; Revol, J. F.; Gray, D. G. Effect of Microcrystallite Preparation Conditions on the Formation of Colloid Crystals of Cellulose. *Cellulose* **1998**, *5*, 19−32.
(39) Arola, S.; Tammelin, T.; Setälä, H.; Tullila, A.; Linder, M. B. Immobilization-Stabilization of Proteins on Nanofibrillated Cellulose Derivatives and Their Bioactive Film Formation. *Biomacromolecules* **2012**, *13*, 594−603.
(40) Li, P.; Sirviö, J. A.; Hong, S.; Ämmälä, A.; Liimatainen, H. Preparation of Flame-Retardant Lignin-Containing Wood Nanofibers Using a High-Consistency Mechano-Chemical Pretreatment. *Chem. Eng. J.* **2019**, *375*, No. 122050.
(41) Isogai, A.; Saito, T.; Fukuzumi, H. TEMPO-Oxidized Cellulose Nanofibers. *Nanoscale* **2011**, *3*, 71−85.
(42) Niinivaara, E.; Faustini, M.; Tammelin, T.; Kontturi, E. Mimicking the Humidity Response of the Plant Cell Wall by Using Two-Dimensional Systems: The Critical Role of Amorphous and Crystalline Polysaccharides. *Langmuir* **2016**, *32*, 2032−2040.
(43) Peresin, M. S.; Kammiovirta, K.; Heikkinen, H.; Johansson, L. S.; Vartiainen, J.; Setälä, H.; Österberg, M.; Tammelin, T. Understanding the Mechanisms of Oxygen Diffusion through Surface Functionalized Nanocellulose Films. *Carbohydr. Polym.* **2017**, *174*, 309−317.
(44) Mougel, J. B.; Adda, C.; Bertoncini, P.; Capron, I.; Cathala, B.; Chauvet, O. Highly Efficient and Predictable Noncovalent Dispersion of Single-Walled and Multi-Walled Carbon Nanotubes by Cellulose Nanocrystals. *J. Phys. Chem. C* **2016**, *120*, 22694−22701.
(45) Reyes, G.; Lundahl, M. J.; Alejandro-Martín, S.; Arteaga-Pérez, L. E.; Oviedo, C.; King, A. W. T.; Rojas, O. J. Coaxial Spinning of All-Cellulose Systems for Enhanced Toughness: Filaments of Oxidized Nanofibrils Sheathed in Cellulose II Regenerated from a Protic Ionic Liquid. *Biomacromolecules* **2020**, *21*, 878−891.
(46) Protopopova, V.; Iyer, A.; Wester, N.; Kondrateva, A.; Sainio, S.; Palomäki, T.; Laurila, T.; Mishin, M.; Koskinen, J. Ultrathin Undoped Tetrahedral Amorphous Carbon Films: The Role of the Underlying Titanium Layer on the Electronic Structure. *Diamond Relat. Mater.* **2015**, *57*, 43−52.
(47) Liimatainen, H.; Sirviö, J.; Sundman, O.; Hormi, O.; Niinimäki, J. Use of Nanoparticular and Soluble Anionic Celluloses in Coagulation-Flocculation Treatment of Kaolin Suspension. *Water Res.* **2012**, *46*, 2159−2166.
(48) Hunter, R. J. *Foundations of Colloid Science*; Oxford University Press: 1986; Vol. *1*.
(49) Bhattacharjee, S. DLS and Zeta Potential - What They Are and What They Are Not? *J. Controlled Release* **2016**, *235*, 337−351.
(50) Oh, S. Y.; Dong, I. Y.; Shin, Y.; Hwan, C. K.; Hak, Y. K.; Yong, S. C.; Won, H. P.; Ji, H. Y. Crystalline Structure Analysis of Cellulose Treated with Sodium Hydroxide and Carbon Dioxide by Means of X-Ray Diffraction and FTIR Spectroscopy. *Carbohydr. Res.* **2005**, *340*, 2376−2391.
(51) Jiang, F.; Hsieh, Y. L. Chemically and Mechanically Isolated Nanocellulose and Their Self-Assembled Structures. *Carbohydr. Polym.* **2013**, *95*, 32−40.
(52) Yu, J.; Grossiord, N.; Koning, C. E.; Loos, J. Controlling the Dispersion of Multi-Wall Carbon Nanotubes in Aqueous Surfactant Solution. *Carbon* **2007**, *45*, 618−623.
(53) Kataura, H.; Kumazawa, Y.; Maniwa, Y.; Umezu, I.; Suzuki, S.; Ohtsuka, Y.; Achiba, Y. Optical Properties of Single-Wall Carbon Nanotubes. *Synth. Met.* **1999**, *103*, 2555−2558.
(54) Niu, F.; Li, M.; Huang, Q.; Zhang, X.; Pan, W.; Yang, J.; Li, J. The Characteristic and Dispersion Stability of Nanocellulose Produced by Mixed Acid Hydrolysis and Ultrasonic Assistance. *Carbohydr. Polym.* **2017**, *165*, 197−204.
(55) Alafogianni, P.; Dassios, K.; Farmaki, S.; Antiohos, S. K.; Matikas, T. E.; Barkoula, N. M. On the Efficiency of UV-Vis Spectroscopy in Assessing the Dispersion Quality in Sonicated Aqueous Suspensions of Carbon Nanotubes. *Colloids Surf., A* **2016**, *495*, 118−124.
(56) Ruderman, G.; Caffarena, E. R.; Mogilner, I. G.; Tolosa, E. J. Hydrogen Bonding of Carboxylic Acids in Aqueous Solutions - UV Spectroscopy, Viscosity, and Molecular Simulation of Acetic Acid. *J. Solution Chem.* **1998**, *27*, 935−948.
(57) Abdul Khalil, H. P. S.; Davoudpour, Y.; Islam, M. N.; Mustapha, A.; Sudesh, K.; Dungani, R.; Jawaid, M. Production and Modification of Nanofibrillated Cellulose Using Various Mechanical Processes: A Review. *Carbohydr. Polym.* **2014**, *99*, 649−665.
(58) Elazzouzi-Hafraoui, S.; Nishiyama, Y.; Putaux, J. L.; Heux, L.; Dubreuil, F.; Rochas, C. The Shape and Size Distribution of Crystalline Nanoparticles Prepared by Acid Hydrolysis of Native Cellulose. *Biomacromolecules* **2008**, *9*, 57−65.
(59) Kontturi, E.; Vuorinen, T. Indirect Evidence of Supramolecular Changes within Cellulose Microfibrils of Chemical Pulp Fibers upon Drying. *Cellulose* **2009**, *16*, 65−74.
(60) Larson, R. G. In Retrospect: Twenty Years of Drying Droplets. *Nature* **2017**, *550*, 466−467.
(61) Klockars, K. W.; Yau, N. E.; Tardy, B. L.; Majoinen, J.; Kämäräinen, T.; Miettunen, K.; Boutonnet, E.; Borghei, M.; Beidler, J.; Rojas, O. J. Asymmetrical Coffee Rings from Cellulose Nanocrystals and Prospects in Art and Design. *Cellulose* **2019**, *26*, 491−506.
(62) Reid, M. S.; Kedzior, S. A.; Villalobos, M.; Cranston, E. D. Effect of Ionic Strength and Surface Charge Density on the Kinetics of Cellulose Nanocrystal Thin Film Swelling. *Langmuir* **2017**, *33*, 7403−7411.
(63) Balducci, A.; Belanger, D.; Brousse, T.; Long, J. W.; Sugimoto, W. Perspective—A Guideline for Reporting Performance Metrics with Electrochemical Capacitors: From Electrode Materials to Full Devices. *J. Electrochem. Soc.* **2017**, *164*, A1487−A1488.
(64) Sainio, S.; Palomäki, T.; Rhode, S.; Kauppila, M.; Pitkänen, O.; Selkälä, T.; Toth, G.; Moram, M.; Kordas, K.; Koskinen, J.; Laurila, T. Chemical Carbon Nanotube (CNT) Forest Grown on Diamond-like Carbon (DLC) Thin Films Significantly Improves Electrochemical

https://doi.org/10.1021/acsanm.1c00774
ACS Appl. Nano Mater. 2021, 4, 5842−5853

Sensitivity and Selectivity towards Dopamine. *Sens. Actuators, B* **2015**, *211*, 177−186.
(65) Redepenning, J.; Anson, F. C. Permselectivities of Polyelectrolyte Electrode Coatings as Inferred from Measurements with Incorporated Redox Probes or Concentration Cells. *J. Phys. Chem. A* **1987**, *91*, 4549−4553.
(66) Shi, M.; Anson, F. C. Some Consequences of the Significantly Different Mobilities of Hydrophilic and Hydrophobic Metal Complexes in Perfluorosulfonated Ionomer Coatings on Electrodes. *Anal. Chem.* **1997**, *69*, 2653−2660.
(67) Thielemans, W.; Warbey, C. R.; Walsh, D. A. Permselective Nanostructured Membranes Based on Cellulose Nanowhiskers. *Green Chem.* **2009**, *11*, 531−537.
(68) Hakalahti, M.; Faustini, M.; Boissière, C.; Kontturi, E.; Tammelin, T. Interfacial Mechanisms of Water Vapor Sorption into Cellulose Nanofibril Films as Revealed by Quantitative Models. *Biomacromolecules* **2017**, *18*, 2951−2958.
(69) Niinivaara, E.; Faustini, M.; Tammelin, T.; Kontturi, E. Water Vapor Uptake of Ultrathin Films of Biologically Derived Nanocrystals: Quantitative Assessment with Quartz Crystal Microbalance and Spectroscopic Ellipsometry. *Langmuir* **2015**, *31*, 12170−12176.
(70) Azzam, F.; Moreau, C.; Cousin, F.; Menelle, A.; Bizot, H.; Cathala, B. Cellulose Nanofibril-Based Multilayered Thin Films: Effect of Ionic Strength on Porosity, Swelling, and Optical Properties. *Langmuir* **2014**, *30*, 8091−8100.

https://doi.org/10.1021/acsanm.1c00774
ACS Appl. Nano Mater. 2021, 4, 5842−5853